The Astrophysical Journal, 576:274–284, 2002 September 1

A COMPARISON OF ^{13}CO AND CS EMISSION IN THE INNER GALAXY

Kristen B. W. McQuinn, Robert Simon, Casey J. Law,[1] James M. Jackson, T. M. Bania, and Dan P. Clemens
Institute for Astrophysical Research, Boston University, 725 Commonwealth Avenue, Boston, MA 02215;
kbw@bu-ast.bu.edu, simonr@chub.bu.edu, jackson@bu-ast.bu.edu, bania@ninkasi.bu.edu, clemens@bu.edu

and

Mark H. Heyer
Five College Radio Astronomy Observatory and Department of Physics and Astronomy, Lederle Graduate Research Tower,
University of Massachusetts, Amherst, MA 01003; heyer@astro.umass.edu
Received 2001 October 4; accepted 2002 May 2

ABSTRACT

We analyze 2 deg^2 of the Galactic plane surveyed in CS $J = 2 \rightarrow 1$ and ^{13}CO $J = 1 \rightarrow 0$ emission lines as a part of the Boston University–Five College Radio Astronomy Observatory Milky Way Galactic Ring Survey. Since the critical density of the CS molecule is large, strong CS emission originates only in dense molecular cloud cores. Yet, because high volume density regions traced by CS also tend to have large column densities, we find that ^{13}CO is just as useful as, and much more efficient than, CS for identifying potential dense, star-forming cores. Sixty-five percent of the star-forming sites in the survey region, selected using color criteria for embedded *IRAS* point sources, are detected as bright ^{13}CO clumps with emission above an integrated intensity of 15 K km s^{-1} (greater than 37 σ). The fraction of those infrared point sources detected as bright CS clumps above 1 K km s^{-1} (greater than 3 σ) is only 35%. The CS/^{13}CO intensity ratio can be used as a measure of gas excitation conditions. We compared the observed CS and ^{13}CO line intensities of the entire 2 deg^2 field as well as the average line ratios from two molecular clouds with very different physical properties. The average intensity ratio for GRSMC 45.46+0.05, a high volume density, star-forming molecular cloud, calculated with a high (26 K km s^{-1}) ^{13}CO flux threshold, is $T_{\rm mb}({\rm CS})/T_{\rm mb}(^{13}{\rm CO}) = 0.17 \pm 0.06$, with a peak value of $\sim$0.5 toward two of the CS emission maxima. The ratio for the same cloud calculated using all ^{13}CO positions with flux above 3 σ is 0.06 ± 0.01. For GRSMC 45.60+0.30, a low-density, quiescent molecular cloud, this ratio is even lower, 0.03 ± 0.01. The average line ratio for the entire 2 deg^2 field is 0.04 ± 0.01, similar to the value for the low-density cloud. Although the CS lines are brightest toward star-forming cores, ubiquitous, low-level CS emission dominates the emission in the survey region. This emission probably originates from subthermally excited, low-density gas.

Subject headings: Galaxy: general — ISM: clouds — ISM: molecules — radio lines: ISM — surveys

1. INTRODUCTION

Molecular gas in the Galaxy is distributed over a broad range of density regimes. Most of the molecular mass resides within the spatially extended, low column and volume density giant molecular clouds (GMCs) and is conventionally traced by the millimeter rotational transitions of ^{12}CO and ^{13}CO and optical/IR extinction measurements (e.g., Carpenter, Snell, & Schloerb 1995; Heyer, Carpenter, & Ladd 1996; Lada, Alves, & Lada 1999). While occupying a small fraction of the volume and mass of GMCs, regions of enhanced density (greater than 10^4 cm^{-3}) are important because these are the sites of star formation. The properties of this dense gas component such as angular momentum, temperature, or turbulent energy regulate the yield of newborn stars. Such dense regions are typically revealed by centimeter- and millimeter-wave transitions of molecules that require high densities for excitation such as NH_3, CS, or HCN (e.g., Ho & Townes 1983; Lada, Bally, & Stark 1991; Paglione, Jackson, & Ishizuki 1997 and references therein).

Wide-field imaging of the dense gas within GMCs provides important constraints to describe the star formation process in the Milky Way because these generate an unbiased census of dense gas. To date, such surveys have been limited, however, to targeted molecular clouds (Lada, Bally, & Stark 1991; Tatematsu et al. 1998) or to sparse sampling along the Galactic plane (Lee, Snell, & Dickman 1990; Helfer & Blitz 1997). When the ratio of HCN or CS to CO intensities is used as an approximate gauge of the physical gas conditions, the central regions of the Galaxy exhibit higher excitation conditions than those elsewhere in the plane and solar neighborhood (Lee et al. 1990; Jackson et al. 1996; Helfer & Blitz 1997; Paglione et al. 1998). In addition, from sparsely sampled, unbiased surveys of HCN and CS emission along the Galactic plane, weak signals are detected along many lines of sight. The $I_{\rm HCN/CO}$ and $I_{\rm CS/CO}$ ratios are lower than those found in dense cores of nearby GMCs (Helfer & Blitz 1997). These lower ratios suggest moderate gas densities.

Because star-forming cores are spatially compact (less than 0.5 pc), it is important that such surveys of dense gas be made with high spatial dynamic range. As part of the Boston University–Five College Radio Astronomy Observatory (BU-FCRAO) Milky Way Galactic Ring Survey (Simon et al. 2001), a new high-resolution, fully sampled ^{13}CO $J = 1 \rightarrow 0$ survey of the 5 kpc molecular ring, the most prominent star-forming structure of our Galaxy (e.g., Robinson et al. 1984), we have observed 2 deg^2 of CS $J = 2 \rightarrow 1$ emission to compare with ^{13}CO $J = 1 \rightarrow 0$ observations of the same field. Such unbiased, fully sampled

---

[1] Harvard-Smithsonian Center for Astrophysics, 60 Garden Street, MS-81, Cambridge, MA 02138; claw@head-cfa.harvard.edu.

imaging surveys can more directly address the origin of extended HCN and CS emission and the spatial and kinematic relationships between the dense cores and the overlying molecular cloud.

We find that ^{13}CO is as useful as CS in identifying potential high-density cores of star-forming regions. Strong ^{13}CO emission correlates well with strong CS emission and with *IRAS* point sources satisfying the color criteria for embedded star-forming regions. ^{13}CO traces even a higher number of these infrared point sources as bright molecular clumps than CS. Moreover, although the strongest CS emission originates from dense, molecular cloud cores, the average CS emission seen in the area surveyed is weak and originates from subthermally excited gas in lower density molecular clouds.

In § 2, we discuss the technical details of the CS/^{13}CO survey. In § 3, we describe our methods of comparing the CS and ^{13}CO emission. In § 4, we discuss the implications of our analysis, which confirms the previous findings by Drdla, Knapp, & van Dishoeck (1989), Liszt (1995), and Helfer & Blitz (1997) concerning the ubiquity of low-level CS emission in unbiased observations of large fields in the Galactic plane.

2. COMPARATIVE SURVEY DATA

The survey observations were obtained with the Five College Radio Astronomy Observatory (FCRAO) 14 m telescope between 1998 December and 1999 May. Two molecular transitions were observed: the CS $J = 2 \rightarrow 1$ transition at 97.981 GHz and the ^{13}CO $J = 1 \rightarrow 0$ transition at 110.201 GHz.[2] The FWHM beam size of the telescope is $46''$ at the ^{13}CO frequency.

The FCRAO 16 element array receiver, SEQUOIA, provided a mean receiver noise temperature of 80 K. Typical system temperatures ranged between 150 and 250 K for both molecular transitions. The spectrometer consisted of 16 autocorrelators, each with a bandwidth of 40 MHz, 512 channels, and a channel spacing for ^{13}CO (CS) of 0.21 (0.24) km s^{-1}. The FWHM velocity resolution is 0.26 (0.29) km s^{-1} for ^{13}CO (CS). The resulting bandwidth of 110 km s^{-1} was sufficient to cover all ^{13}CO and CS emission at positive local standard of rest (LSR) velocities for Galactic longitudes above 40°.

The spectra were calibrated using a vane to switch between emission from the sky and an ambient temperature load. All intensities are reported on a main-beam brightness temperature scale, $T_{\rm mb}$, using the main-beam efficiency values of $\eta_{\rm mb} = 0.50$ for CS and $\eta_{\rm mb} = 0.48$ for ^{13}CO as derived from observations of Jupiter.

The survey observations were obtained using a position-switching mode where four consecutive array pointings toward target regions shared the same off-source reference integration. Integration times for one target pointing ranged between 20 and 60 s. The resulting spectra have a mean per channel noise level (rms main-beam temperature) of 0.48 K for ^{13}CO and 0.36 K for CS.

Sky reference positions free of ^{12}CO $J = 1 \rightarrow 0$ emission were selected from the Columbia survey maps (Dame, Hartmann, & Thaddeus 2001). These potential off-source reference positions were chosen to be as close as possible to both the Galactic plane and our target positions. They were then checked for emission in ^{13}CO by position-switched observations against positions from the Columbia survey known to be free of emission in ^{12}CO to an rms noise level of 0.05 K (main-beam temperature per 0.65 km s^{-1} channel) in an $8'$ beam. No ^{13}CO emission was found toward these off-source positions above a noise level of $\Delta T_{\rm mb} \sim 0.15$ K.

3. RESULTS

3.1. *Maps of* ^{13}CO *and* CS *Emission*

A 2 deg^2 field, $l = 44\fdg3$ to $46\fdg3$ and $b = -0\fdg5$ to $0\fdg5$, was observed. The data set consists of spectra for a total of $\sim$62,000 positions obtained on a $22''$ grid for each transition. The 2 deg^2 of sky mapped for this comparative survey are shown in Figure 1. In Figure 1*a*, the CS $J = 2 \rightarrow 1$ data are shown in the gray scale. Figure 1*b* displays the same CS data as contours overlaid on the gray-scale map of ^{13}CO $J = 1 \rightarrow 0$ emission (Simon et al. 2001).

These maps show the integrated intensity within a velocity range of $V_{\rm LSR} = -5$ to 80 km s^{-1}. The maps were constructed following the masked moment procedure (Adler et al. 1992), which filters out noise and spikes in the data. The intensity of each channel was compared to the intensity of its neighboring channels in (l, b, V). If the intensity of the channel and the intensities of its neighbors were greater than some temperature threshold, the intensity of this channel was added to the total integrated intensity at this position and used in the map. Since the noise is not entirely uniform across the mapped region, we used a temperature threshold per velocity channel of 0.52 K for ^{13}CO and 0.40 K for CS, i.e., slightly higher than the average rms noise temperatures.

In Figure 1*a*, we superposed objects from the *IRAS* point-source catalog on top of the CS emission. The large symbols represent those infrared point sources that have far-infrared colors that are typical for embedded star-forming regions according to the selection criteria of Wouterloot et al. (1990): (1) the sources are recorded as detections at 25, 60, and 100 μm in the point-source catalog, (2) the flux at 25 μm is greater than that at 12 μm, and (3) the ratios of $\log(\nu S)$ in *IRAS* band *j* to band *i* (1, 2, 3, and 4, corresponding to 12, 25, 60, and 100 μm, respectively) are such that $0 < R_{23} < 1.5$ and $-1 < R_{34} < (0.261 + 0.227 R_{23})$.

There are a few previously identified objects in the 2 deg^2 surveyed that are labeled in Figure 1 as Galactic Ring Survey Molecular Clouds (GRSMCs; Simon et al. 2001), according to their positions in the survey. The molecular cloud complex GRSMC 45.46+0.05 at a distance of 6.0 kpc (e.g., Lockman 1989; Simon et al. 2001) contains a collection of H II regions marking an area of intense star formation activity. The source GRSMC 45.70−0.40 is a similar cloud at the same distance with strong CS and ^{13}CO emission and star-forming activity. Finally, too faint to be clearly visible in the ^{13}CO moment image, GRSMC 45.60+0.30 is a nearby (1.8 kpc) quiescent molecular cloud (Simon et al. 2001; Jackson et al. 2002).

Figure 2 displays the same field of view with the CS data smoothed to an FWHM angular resolution of $4'$ ($2'$ grid) and the same *IRAS* point sources plotted on top of the image. The smoothing improves the signal-to-noise ratio, revealing low-level, extended CS emission. Figure 2 shows

---

[2] The CS $J = 2 \rightarrow 1$ and ^{13}CO $J = 1 \rightarrow 0$ data are available in FITS format at http://www.bu.edu/GRS.

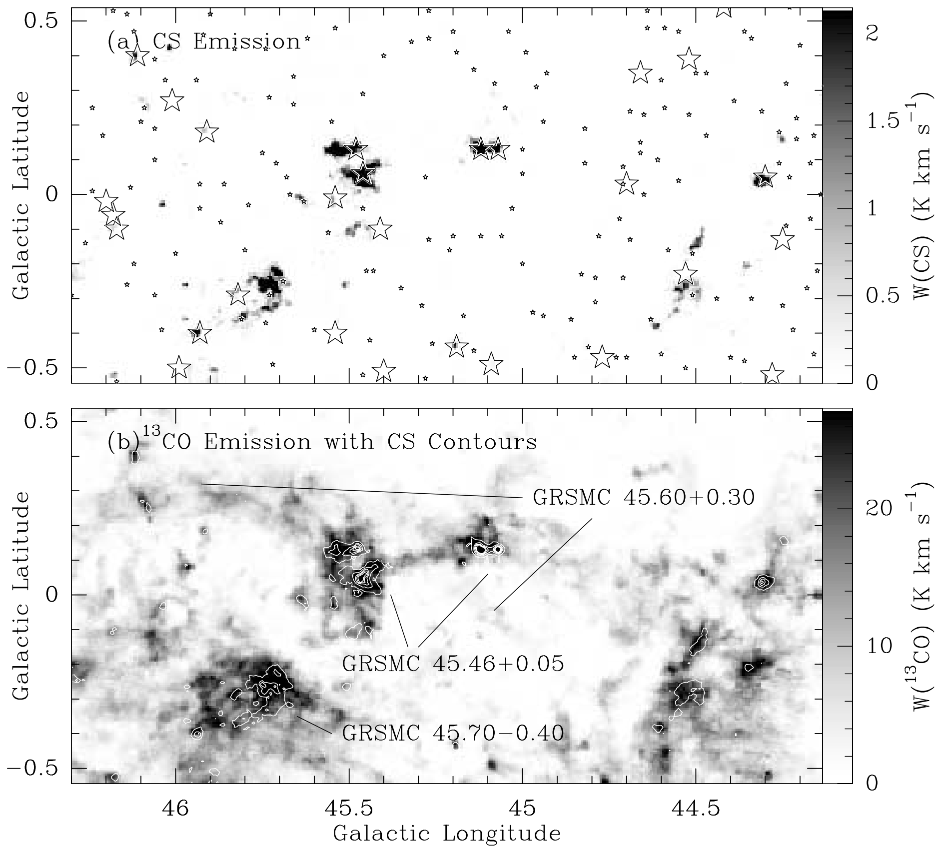

FIG. 1.—Integrated intensity maps of ^{13}CO and CS emission for the LSR velocity range −5 to 80 km s^{-1}. (*a*) CS $J = 2 \rightarrow 1$ emission in gray scale for the 2 deg^2 region surveyed along the Galactic plane. The stretch of the gray scale was chosen to show the faint emission and does not reach the peak flux of 21.5 K km s^{-1}. (*b*) Gray scale of the ^{13}CO $J = 1 \rightarrow 0$ emission from the same region with CS emission overlaid as contours at 0.5–10.0 K km s^{-1} in steps of 2.4 K km s^{-1}. Large and small stars mark the positions of *IRAS* point sources in the survey field. The large star symbols are those *IRAS* point sources that meet the criteria for embedded star formation as given by Wouterloot et al. (1990).

that CS emission traces the same molecular clouds as ^{13}CO throughout the 2 deg^2 surveyed.

3.2. CS *and* ^{13}CO *Integrated Intensities*

To increase the signal-to-noise ratio for the following comparison of integrated line intensities, we smoothed the CS and ^{13}CO data to an angular resolution of 4′ on a 2′ grid. Of the 2015 spectra for each CS and ^{13}CO position in the smoothed data sets, 75% of the CS spectra have emission above the 3 σ noise level within the velocity range from 0 to 80 km s^{-1}, while the ^{13}CO line is detected above the 3 σ level toward all grid positions in the field. To quantify at what integrated intensity level this emission is detected, we show

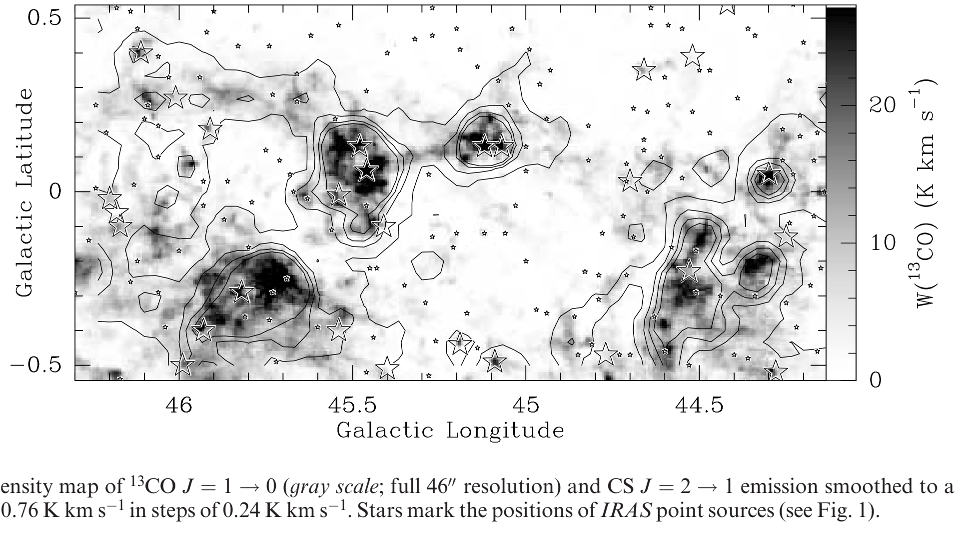

FIG. 2.—Integrated intensity map of ^{13}CO $J = 1 \rightarrow 0$ (*gray scale*; full 46″ resolution) and CS $J = 2 \rightarrow 1$ emission smoothed to a 4′ beam (*contours*). The contours are from 0.05 to 0.76 K km s^{-1} in steps of 0.24 K km s^{-1}. Stars mark the positions of *IRAS* point sources (see Fig. 1).

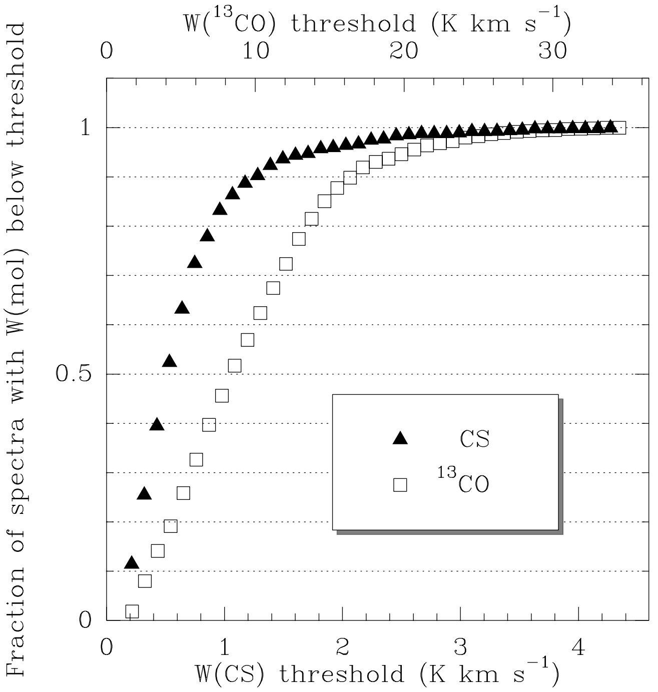

FIG. 3.—Plot of the fraction of smoothed (4′ beam, 2′ grid) spectra with total integrated intensity ($V_{\rm LSR}$ from 0 to 80 km s^{-1}) above the 3 σ noise level but below an integrated intensity threshold, as a function of this threshold. CS data are represented by filled triangles, ^{13}CO data by open squares. Since the ^{13}CO integrated intensities are generally much higher than those for CS, the plot contains two differently stretched integrated intensity threshold axes for *W*(CS) (*bottom*) and *W*(^{13}CO) (*top*).

in Figure 3 the fraction of spectra for the CS and ^{13}CO transitions with total integrated intensity (velocity range from 0 to 80 km s^{-1}) below certain threshold values.

Nearly 85% of the CS spectra with detected emission have a total integrated intensity below 1 K km s^{-1} [which is only 23% of the peak *W*(CS)]. Above 1 K km s^{-1}, the integrated intensity for the remaining 15% of spectra increases rapidly. These are spectra where, because of the high critical density of CS, the CS excitation is enhanced in the higher density cores of the survey region.

Almost 90% of the ^{13}CO spectra have total integrated intensities below 15 K km s^{-1} (which is almost 50% of the peak ^{13}CO value), and the integrated line intensities are more evenly distributed over a wider range in *W*(^{13}CO) than for CS. Above ~15 K km s^{-1}, ^{13}CO shows a rapid increase of integrated intensities for the remaining 10% of spectra, very similar to CS. From Figures 1 and 2 it is evident that the corresponding spectra are toward the same high-density regions as traced by CS that are picked out by ^{13}CO since they also have high column densities.

Figures 2 and 3 show that low-level CS emission is ubiquitous in the survey region and dominates the total CS flux.

The relationship between CS and ^{13}CO integrated intensity was further studied by comparing the emission detected in 10 km s^{-1} wide bins of the smoothed data sets in order to look for possible correlations between the CS and ^{13}CO integrated intensities. We divided the spectra into 10 km s^{-1} bins, ranging from 0 to 80 km s^{-1}. For the case of several clouds along the same line of sight at different velocities, this procedure separates the clouds.

The total integrated intensity per bin was calculated for each position of the smoothed data sets using a method similar to that employed in making the moment maps in Figures 1 and 2. If a 0.26 km s^{-1} wide spectral channel within a particular 10 km s^{-1} wide bin had emission above the 3 σ noise level of the corresponding smoothed spectrum and the adjacent velocity channels also had emission above 3 σ, we added the intensity of that channel to the total integrated intensity of that velocity bin. Both the CS and ^{13}CO spectral channels for each position were required to meet this strict criterion, which was chosen to ensure that only emission well above the noise level was counted.

Figure 4 plots the CS integrated intensity, *W*(CS), versus the ^{13}CO integrated intensity, *W*(^{13}CO), for all 10 km s^{-1} wide velocity bins of the data. Most of the points in Figure 4 correspond to sky positions with low CS integrated intensities [$W({\rm CS}) < 1$ km s^{-1}]. This emission probably originates from subthermally excited CS in low-density gas (see § 4.2). There are no pairs [*W*(^{13}CO), *W*(CS)] in the plot showing both strong CS integrated intensity [$W({\rm CS}) \gtrsim 1$ K km s^{-1}] *and* weak ^{13}CO integrated intensity [$W(^{13}{\rm CO}) \lesssim 10$ K km s^{-1}]. This confirms our assessment of Figures 1 and 2 that all strong CS emission originates from areas that also show strong ^{13}CO emission. The correlation between strong ^{13}CO and CS emission simply reflects the fact that high-density cores are also expected to have high column densities. Additionally, all features with strong ^{13}CO emission also exhibit strong CS emission. Nearly all points in the graph with strong ^{13}CO and CS emission originate from the velocity range $V_{\rm LSR} = 50$–70 km s^{-1}, which corresponds to the tangent point velocity range at this Galactic longitude. Many of these points are associated with the star-forming region GRSMC 45.46+0.05.

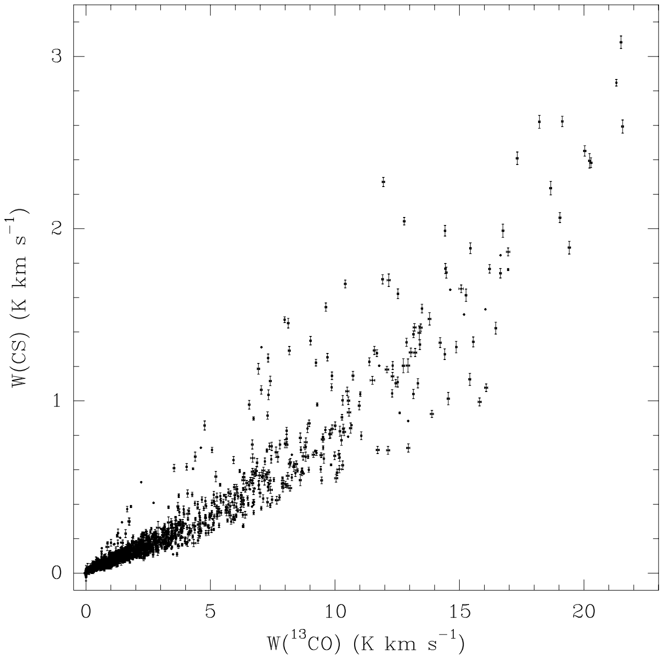

FIG. 4.—Plot of CS versus ^{13}CO integrated intensities calculated across 10 km s^{-1} bins for all positions in the smoothed data sets. Channels with emission greater than 3 σ whose neighboring channels also had emission above 3 σ contributed to the total integrated intensity per bin. The error bars were calculated from the rms of each spectrum and the number of channels contributing to the total integrated intensity of a velocity bin.

3.3. CS *and* ^{13}CO *Line Emission Ratios*

Interstellar gas physical properties derived using molecular tracers that have, e.g., different relative abundances or different responses to excitation conditions can vary as a function of the volume size over which a given property is calculated. Below, we estimate this variation for the CS/^{13}CO ratio.

3.3.1. *The Entire Field*

All 62,000 ^{13}CO and CS spectra from the 2 deg^2 surveyed were accumulated to form single, average spectra. These spectra and their $T_{\rm mb}({\rm CS})/T_{\rm mb}(^{13}{\rm CO})$ ratio spectrum are shown in Figure 5. The ratio spectrum was calculated after applying a 3 σ cutoff to the average CS and ^{13}CO spectra. Error bars to the ratio were determined from the rms noise level of the two averaged spectra. In the following, final intensity ratios for the selected fields are given as weighted mean and standard deviation determined from spectral channels with significant emission in the averaged spectra. Although several distinct emission features can be identified in the ^{13}CO spectrum, only the two most prominent features have significant CS emission. After applying the 3 σ cutoff across the entire −5 to 80 km s^{-1} LSR velocity range, only between $V_{\rm LSR}$ = 23–28 km s^{-1} and $V_{\rm LSR}$ = 48–70 km s^{-1} is there sufficient CS emission to determine a reliable intensity ratio. We find a mean CS/^{13}CO intensity ratio in the entire field of 0.04 ± 0.01.

3.3.2. *The Star-forming Region GRSMC 45.46+0.05*

Within the velocity ranges showing significant emission in CS and ^{13}CO, we identified two clouds having very different physical properties and levels of star-forming activity. The first, shown in Figure 6*a* taken from Simon et al. (2001), emits in the range $V_{\rm LSR}$ = 50–70 km s^{-1} and contains the most intense CS and ^{13}CO emission found in the 2 deg^2 region. This emission is associated with the molecular cloud complex GRSMC 45.46+0.05, which is known to contain three H II regions (Lockman 1989).

In order to determine the CS to ^{13}CO intensity ratio for the whole cloud, we first averaged all ^{13}CO spectra with peak fluxes above the 3 σ level within the boundaries $l = 44.^\circ95$–$45.^\circ70$ and $b = -0.^\circ15$ to $0.^\circ30$ for $V_{\rm LSR}$ between 50 and 70 km s^{-1} (those positions are shown in Fig. 6*b*). CS spectra toward the positions of the selected ^{13}CO spectra were also averaged. The resulting spectra and the intensity ratio spectrum, calculated after applying a 3 σ cutoff to the average CS spectrum, are shown in Figure 7. The brightest velocity component seen in ^{13}CO emission is centered at $V_{\rm LSR}$ = 59 km s^{-1} with a peak $T_{\rm mb}(^{13}{\rm CO}) = 1.3$ K and peak $T_{\rm mb}({\rm CS}) = 0.08$ K. The CS/^{13}CO main-beam temperature ratio is almost constant across the whole range $V_{\rm LSR}$ = 50–70 km s^{-1}. The weighted mean ratio of $T_{\rm mb}({\rm CS})/T_{\rm mb}(^{13}{\rm CO})$ is 0.06 ± 0.01.

In a second approach, we averaged all ^{13}CO spectra with peak fluxes greater than 26 K km s^{-1} (∼27 σ) within the above-defined cloud boundaries and the velocity range of 50–70 km s^{-1} (those positions are shown in Fig. 6*c*). The resulting spectra and the intensity ratio spectrum are shown in Figure 8. Although the value of 26 K km s^{-1} is arbitrary, the CS integrated intensity contours plotted on top of the selected ^{13}CO positions (Fig. 6*c*) illustrate that this flux threshold in fact isolates the higher density environments of the star-forming molecular cloud as traced by strong CS emission. As before, CS spectra toward the same positions as defined by the selected ^{13}CO spectra were averaged and plotted with the resulting ^{13}CO spectrum. The peak main-beam temperatures for the core average spectra are $T_{\rm mb}(^{13}{\rm CO}) = 5.3$ K and $T_{\rm mb}({\rm CS}) = 1.0$ K. Figure 8*b* shows the intensity ratio spectrum for the cloud core regions. A 3 σ

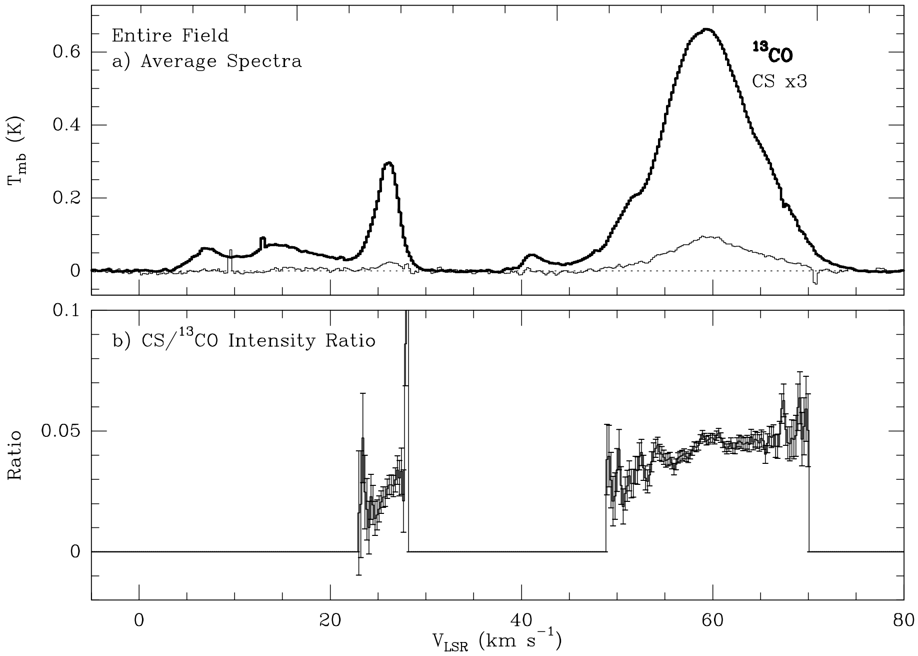

FIG. 5.—^{13}CO and CS spectra and intensity ratio spectrum for the entire 2 deg^2 surveyed. (*a*) Average ^{13}CO spectrum (*thick line*) and average CS spectrum (*thin line*) multiplied by 3. (*b*) Average CS/^{13}CO intensity ratio spectrum for the entire field.

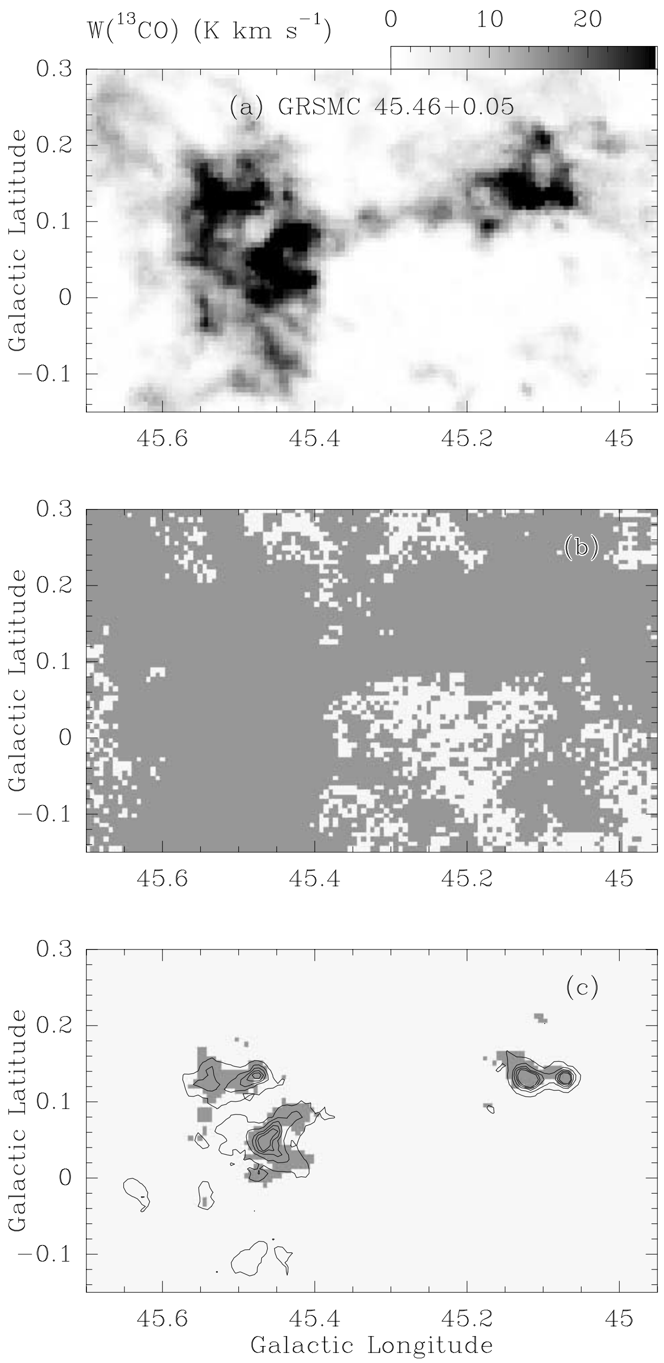

FIG. 6.—(*a*) ^{13}CO integrated intensity map of the star-forming molecular cloud in the survey region GRSMC 45.46+0.05 (adopted from Simon et al. 2001). The cloud emits over a velocity range of $V_{\rm LSR}$ = 50–70 km s^{-1}. (*b*) Positions with ^{13}CO spectra having peak fluxes above the 3 σ level between $V_{\rm LSR}$ = 50 and 70 km s^{-1} are shown as dark pixels. (*c*) Same as (*b*) for ^{13}CO fluxes above 26 K km s^{-1}. For comparison, the CS integrated intensity contours from Fig. 1*b* are overlaid. The lack of ^{13}CO pixels inside the CS contours is due to the high ^{13}CO threshold. The spectra toward the positions highlighted in (*b*) and (*c*) are used to compute the average spectra shown in Figs. 7 and 8.

cutoff was applied to the average CS spectrum before the ratio spectrum was determined. The ratio changes smoothly across the principal Gaussian part of this feature, ranging from 0.09 at 55 km s^{-1} to a maximum of 0.24 at 64 km s^{-1}. Across the whole range $V_{\rm LSR}$ = 50–70 km s^{-1}, the weighted mean ratio is 0.17 ± 0.06.

3.3.3. *Peak* CS *Emission Ratios*

We selected spectra toward the emission peaks of the four brightest CS clumps in the star-forming cloud GRSMC 45.46+0.05 easily seen in Figure 6*c* to determine the peak CS/^{13}CO intensity ratios observed in the survey region. We find peak $T_{\rm mb}({\rm CS})/T_{\rm mb}(^{13}{\rm CO})$ values of 0.5–0.6 in the velocity channels around the line center of spectra toward the two prominent clumps (see Fig. 1) at $(l, b) = (45\overset{\circ}{.}07,\ 0\overset{\circ}{.}13)$ and $(l, b) = (45\overset{\circ}{.}47,\ 0\overset{\circ}{.}14)$. The weighted mean of $T_{\rm mb}({\rm CS})/T_{\rm mb}(^{13}{\rm CO})$ for the two positions using only velocity channels with a ratio higher than 0.4 is 0.49 ± 0.07.

3.3.4. *The Quiescent Cloud GRSMC 45.60+0.30*

The second prominent emission feature in the average ^{13}CO and CS spectra lies in the velocity range $V_{\rm LSR}$ = 23–28 km s^{-1}, corresponding to a distance of only 1.8 kpc. The bulk of this emission is associated with the quiescent molecular cloud GRSMC 45.60+0.30, shown in Figure 9*a* (Simon et al. 2001), which is located along the same line of sight as GRSMC 45.46+0.05. The filamentary structure of GRSMC 45.60+0.30 has considerably weaker emission compared to GRSMC 45.46+0.05 and is associated with a much larger area ($l = 44\overset{\circ}{.}8$–$46\overset{\circ}{.}2$, $b = -0\overset{\circ}{.}5$ to $0\overset{\circ}{.}5$) on the sky. The emission from GRSMC 45.60+0.30 is easily separable from other clouds since it is well isolated in velocity. In calculating the average spectra, a flux limit criterion of $T_{\rm mb}(^{13}{\rm CO}) > 3\ \sigma$ for all channels from $V_{\rm LSR}$ = 20–30 km s^{-1} was used. As for GRSMC 45.46+0.05, a spatially coincident CS spectrum was chosen for each selected ^{13}CO position and averaged. Those positions are shown in Figure 9*b*. The resulting spectra are shown in Figure 10.

The average ^{13}CO spectrum has a Gaussian shape with a peak $T_{\rm mb}(^{13}{\rm CO})$ of 1.08 K. Since the solid angle of this cloud is so great, we were able to average a large number of spectra and therefore extract the very faint CS emission associated with the quiescent cloud. The peak temperature of the average CS spectrum is $T_{\rm mb}({\rm CS}) = 0.03$ K. After applying a 3 σ cutoff to the CS data, we found that the intensity ratio spectrum for this cloud has a weighted mean of 0.03 ± 0.01, which is among the lowest intensity ratios detected in the survey region.

Nowhere in GRSMC 45.60+0.30 do we detect any ^{13}CO signal above the 9 K km s^{-1} (13 σ) level, and CS emission is weak throughout the cloud, making an analysis similar to that toward the star-forming cores in GRSMC 45.46+0.05 impossible. Together with the fact that there is no sign of star formation, the low flux levels suggest that the densities and excitation temperatures even for the more massive clumps in this cloud are rather low. From the ^{13}CO integrated line intensity we can estimate the H_2 column density for the cloud. We assume for GRSMC 45.60+0.30 that the ^{13}CO emission is optically thin and has a rotational temperature of ~10 K, typical for a quiescent cloud. An estimate of the H_2 column density is given by $N({\rm H_2}) = 4.92 \times 10^{20} T_{\rm mb} \Delta V$ (Simon et al. 2001), where ΔV is the FWHM line width in kilometers per second. Assuming a beam-filling factor of unity and $W(^{13}{\rm CO}) \sim 3$ K km s^{-1} (Fig. 9), a typical beam-averaged H_2 column density for this cloud is (1–2) × 10^{21} cm^{-2}. Using a typical clump size for this cloud of 0.7 pc (Simon et al. 2001) as line-of-sight depth, the corresponding H_2 volume density is 10^3 cm^{-3}, which confirms the categorization of GRSMC 45.60+0.30 as a low-density molecular cloud. A slightly higher temperature,

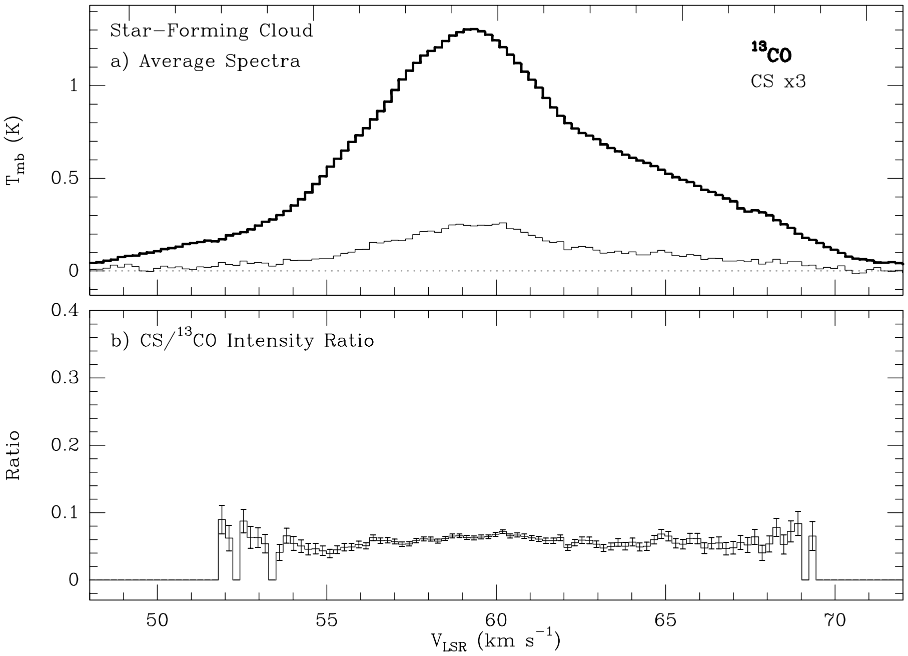

FIG. 7.—^{13}CO and CS spectra and intensity ratio spectrum for GRSMC 45.46+0.05 using all positions with ^{13}CO emission above the 3 σ level. (*a*) Average ^{13}CO spectrum (*bold line*) and average CS spectrum (*thin line*) multiplied by 3. (*b*) Average CS/^{13}CO intensity ratio spectrum.

which is possible in the low column density regime of $A_V \sim 1$–2 mag, will not change the above column density and density estimates by a significant factor (assuming an excitation temperature of 20 K increases the column density by 40%).

The intensity ratios for the individual fields discussed in this section are summarized in Table 1.

4. DISCUSSION

4.1. *The Utility of* ^{13}CO *as a Tracer of Dense Molecular Gas and Star Formation*

Figures 1 and 2 show that the distributions of the ^{13}CO and CS integrated intensities are very similar. Those figures also show that many bright ^{13}CO and CS emission features

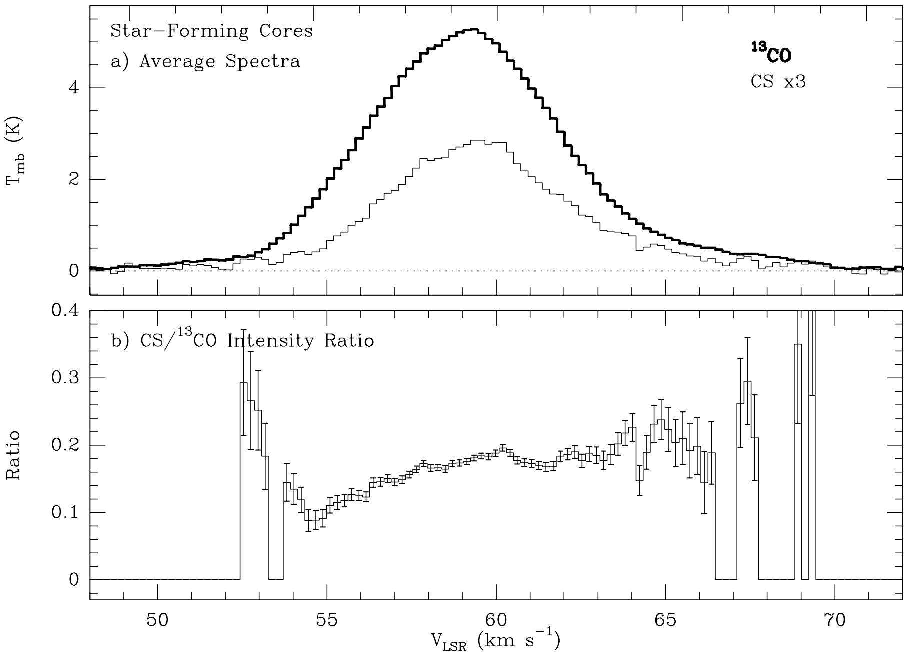

FIG. 8.—^{13}CO and CS spectra and intensity ratio spectrum for the bright emission regions in GRSMC 45.46+0.05 using only positions with ^{13}CO emission above 26 K km s^{-1}. The vertical scale and panel descriptions are the same as for the plots in Fig. 7.

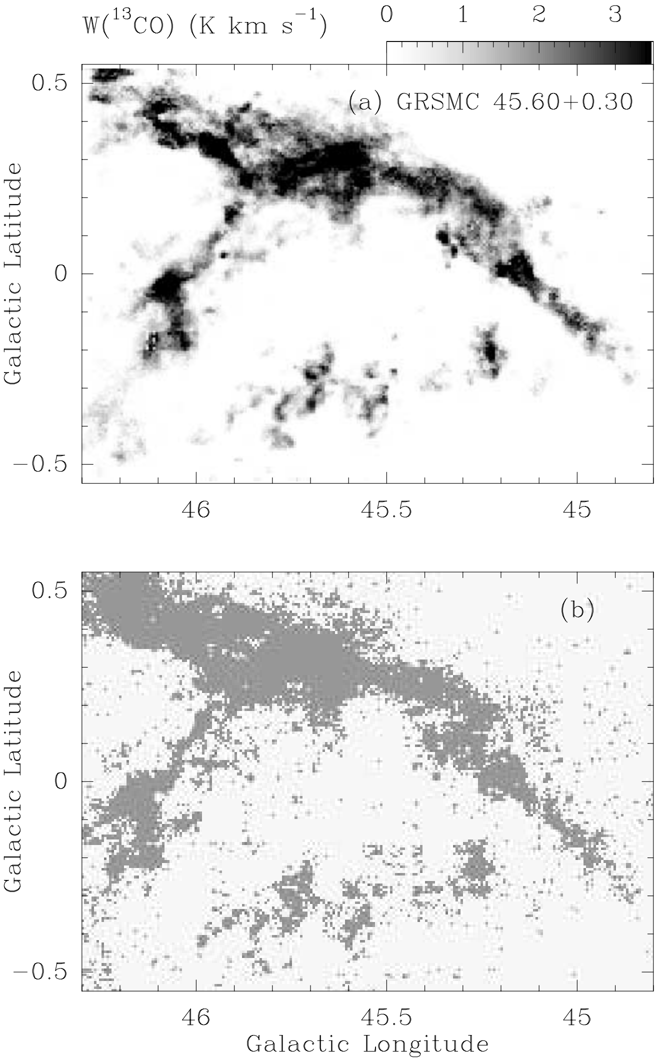

FIG. 9.—(*a*) ^{13}CO integrated intensity maps of the low-density, quiescent molecular cloud in the survey region GRSMC 45.60+0.30 (adopted from Simon et al. 2001). The cloud emits over a velocity range of $V_{\rm LSR} = 23$–28 km s^{-1}. (*b*) Positions with ^{13}CO spectra having peak fluxes above the 3 σ level between $V_{\rm LSR} = 23$ and 28 km s^{-1} are shown as dark pixels. The spectra toward these positions are used to compute the average spectra shown in Fig. 10.

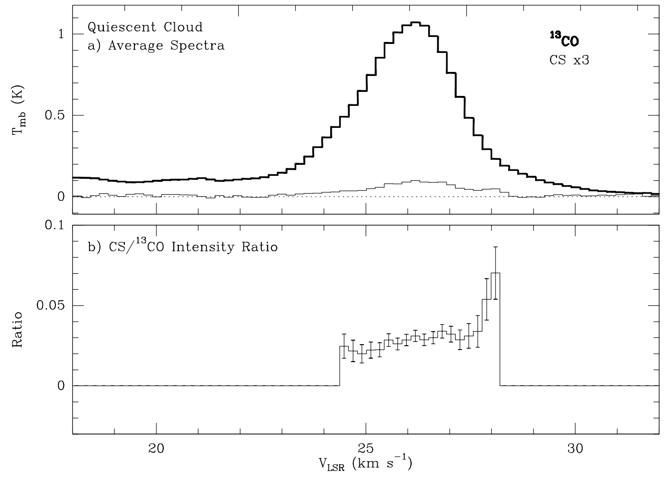

FIG. 10.—^{13}CO and CS spectra and intensity ratio spectrum for GRSMC 45.60+0.30 using all positions with ^{13}CO emission above the 3 σ level. (*a*) Average ^{13}CO spectrum (*thick line*) and average CS spectrum (*thin line*) multiplied by 3. (*b*) Average CS/^{13}CO intensity ratio spectrum for GRSMC 45.60+0.30.

are associated with *IRAS* point sources. Many *IRAS* point sources in the survey region, however, are not associated with bright molecular clumps or molecular emission at all. Those sources may be foreground or evolved stars, cold clumps, or extragalactic. In order to quantify how the molecular line emission correlates with star formation, we isolated 28 *IRAS* point sources fulfilling the criteria for embedded star-forming regions (Wouterloot et al. 1990) and plotted them as large star symbols in Figures 1*a* and 2.

Over 90% of these 28 *IRAS* point sources have ^{13}CO clump counterparts with emission above the 3 σ GRS noise floor. Sixty-five percent of those infrared point sources are detected as bright ^{13}CO clumps with an integrated line intensity above 15 K km s^{-1} [greater than 37 σ, corresponding to $N(\mathrm{H_2}) = 7.4 \times 10^{21}$ cm^{-2} using the assumptions given in the previous section], which was shown in § 3.2 to be the threshold value enclosing ∼10% of the ^{13}CO-emitting area. For CS, only 50% of the selected point-source positions have clump counterparts with emission above the noise of our data and 35% of the star formation candidates are detected as bright CS clumps above 1 K km s^{-1} (greater than 3 σ), the CS integrated intensity threshold corresponding to a ^{13}CO integrated intensity of 15 K km s^{-1} in Figures 3 and 4.

To summarize, nowhere in the survey region do we detect any distinct dense, potentially star-forming core that is seen exclusively in CS since large columns of gas are expected to harbor high-density cores. Moreover, there are even a few *IRAS* point sources tracing potential star formation that are seen in ^{13}CO emission but not in CS emission. When smoothed to an FWHM angular resolution of 4′ (Fig. 2), the weaker CS emission follows the ^{13}CO emission seen from regions with presumably lower density gas. Even for these lower surface brightness features, CS emission always correlates well with ^{13}CO emission.

The CS-^{13}CO relationship seen in Figure 4, where all features with bright CS emission show correspondingly bright ^{13}CO emission, is a manifestation of the similarity of ^{13}CO and CS emission. The slope of $W(\mathrm{CS})/W(^{13}\mathrm{CO})$ in Figure 4 changes from ∼0.06 to ∼0.18 at a ^{13}CO integrated intensity

TABLE 1

SUMMARY OF CS/^{13}CO INTENSITY RATIOS FOR THE DIFFERENT REGIONS

Region	Ratio
Entire Field (3 σ)[a]	0.04 ± 0.01
Quiescent Cloud GRSMC 45.60+0.30 (3 σ)[b]	0.03 ± 0.01
Star-forming Cloud GRSMC 45.46+0.05	
3 σ[b]	0.06 ± 0.01
27 σ[c]	0.17 ± 0.06
Emission Peaks[d]	0.49 ± 0.07

[a] Ratio calculated from ^{13}CO and CS spectra averaged over the whole region after applying a 3 σ cutoff to the averaged spectra.

[b] Ratio calculated using positions with ^{13}CO flux above 3 σ and applying a 3 σ cutoff to the averaged spectra.

[c] Ratio calculated using positions with ^{13}CO flux above 26 K km s^{-1} and applying a 3 σ cutoff to the averaged spectra.

[d] Average ratio for velocity channels with a ratio higher than 0.4 toward the positions of two CS peaks (see text).

around 10 K km s^{-1}. This change in the integrated intensity ratios may be due to several factors acting together. The molecular gas producing the brighter emission toward the cores of the clouds is likely to have volume densities approaching the critical density of the CS transition. This scenario is supported by the correlation between bright CS emission and star-forming molecular cloud cores containing embedded *IRAS* point sources and H II regions. Because these star-forming cores are internally heated, here the CS line traces not only denser but also warmer gas. Although the CS transitions are not likely to be thermalized, the higher gas temperature certainly will result in a locally higher line temperature. Thus, higher gas temperatures inside the clumps would also explain the observed correlation between the brightest CS clumps and embedded *IRAS* point sources. The ^{13}CO line, on the other hand, becomes optically thick at a lower H_2 column density compared to CS and hence traces a colder layer in a high-density, star-forming core. Both effects produce higher CS/^{13}CO ratios and hence a steepening in the slope of the data shown in Figure 4 for large integrated line intensities.

The results from our study are similar to those from a previous study of ^{13}CO, C^{18}O $J = 1 \rightarrow 0$, and CS $J = 2 \rightarrow 1$ emission toward the dark cloud IC 5146 conducted by Lada et al. (1994). They find a linear correlation of integrated molecular line intensities with visual extinction for the optically thin C^{18}O and the high density–tracing CS transition, while the ^{13}CO fluxes show a similar correlation only for $A_V < 5$ mag. Above ~5 mag of visual extinction, the ^{13}CO integrated line intensities flatten, presumably as the $J = 1 \rightarrow 0$ line starts to saturate. An A_V of 5 mag corresponds to a molecular hydrogen column density of $N(H_2) \simeq 5 \times 10^{21}$ cm^{-2}, using the standard conversion from Bohlin, Savage, & Drake (1978) and assuming that all hydrogen is in molecular form. Using the assumptions from the previous section, this column density translates into an integrated ^{13}CO line intensity of ~10 K km s^{-1}, exactly the same integrated intensity where the slope of the $W(\mathrm{CS})/W(^{13}\mathrm{CO})$ ratio in Figure 4 steepens. Moreover, excitation models (Stutzki & Winnewisser 1985; see also § 4.2) show that this column density corresponds to a ^{13}CO $J = 1 \rightarrow 0$ line opacity of about unity. Hence, the change in the slope in Figure 4 most likely results from the saturation of the ^{13}CO line at $A_V > 5$ mag. For the low column density, i.e., low-A_V regime, Lada et al. (1994) find a $W(\mathrm{CS})/W(^{13}\mathrm{CO})$ ratio of ~0.06, in excellent agreement with our results for the average large-scale, low intensity threshold values for GRSMC 45.46+0.05, GRSMC 45.60+0.30, and the entire field.

An alternative explanation for the observed slopes in Figure 4 is that the weak and diffuse CS emission originates from unresolved, thermalized clumps. In regions of higher column density, ^{13}CO becomes optically thick and saturates while CS becomes brighter because of more clumps along the line of sight and less beam dilution. As we will see from the excitation analysis in § 4.2, the observed low ratios of $T_{\mathrm{mb}}(\mathrm{CS})/T_{\mathrm{mb}}(^{13}\mathrm{CO})$ for the diffuse emission are inconsistent with this hypothesis.

In order to compare the brightest clumps in the CS and ^{13}CO full-resolution data on a one-to-one basis, we ran the clump-finding algorithm GAUSSCLUMPS (Stutzki & Güsten 1990). GAUSSCLUMPS models the observed (l, b, V) data as discrete Gaussian-shaped clumps. The results of this analysis show that all bright CS clumps are associated with bright ^{13}CO clumps that are spatially more extended than their CS counterparts. This is expected if CS traces higher density material and ^{13}CO becomes saturated in the outer envelopes of the clumps. All CS clumps containing *IRAS* point sources have corresponding bright ^{13}CO clumps. The *GAUSSCLUMPS* results also confirm that a few bright ^{13}CO clumps associated with *IRAS* point sources do not exhibit CS emission above the sensitivity limit of our survey.

We conclude that high ^{13}CO integrated line intensities trace high column densities ($A_V > 5$ mag) very well and that ^{13}CO alone is a reliable probe for finding potentially dense, star-forming cores. *Since dense molecular cores have large column densities, strong* ^{13}CO *emission reveals possible dense star-forming regions just as effectively as the high volume density–tracing* CS *emission.* In addition, because CS emission is typically 5–20 times fainter than ^{13}CO emission, CS requires much longer telescope integration times to achieve comparable signal-to-noise ratios. Consequently, observing the ^{13}CO $J = 1 \rightarrow 0$ line is much more efficient since it picks out potential star-forming cores, which then can be studied with CS or other high-density tracers, while also providing a census of the lower column density molecular material.

4.2. *The* CS/^{13}CO *Intensity Ratio as a Measure of Volume Density*

The two molecular clouds studied in detail here, GRSMC 45.46+0.05 (Figs. 7 and 8) and GRSMC 45.60+0.30 (Fig. 10), bracket the range of physical conditions found in the 2 deg^2 of the survey. GRSMC 45.46+0.05 is a dense and active cloud, whereas GRSMC 45.60+0.30 is a low-density, quiescent cloud. From analyzing the average spectra of these two clouds, we conclude that the CS/^{13}CO intensity ratio can be used to characterize qualitatively the physical conditions of the source. We posit that a high intensity ratio corresponds to CS emission from dense, potentially star-forming cores and a low intensity ratio is a result of subthermal CS excitation in lower density molecular clouds. This hypothesis is supported by the results of a line escape probability model (Stutzki & Winnewisser 1985) applied to the ^{13}CO and CS transitions. The model is based on radiative transfer in a homogeneous, spherical cloud. We used collisional rate coefficients from Flower & Launay (1985) for ^{13}CO and Green & Chapman (1978) for CS. Abundance ratios for ^{12}CO/^{13}CO of 45 (Langer & Penzias 1990), ^{12}CO/H_2 of 8×10^{-5} (Blake et al. 1987), and CS/H_2 of 2×10^{-9} (Graedel, Langer, & Frerking 1982; Prasad & Huntress 1982) were assumed.

Because the ^{12}CO line is typically optically thick and thermalized, it is a good measure of the kinetic temperature for a homogeneous cloud in the absence of internal or external heating sources. We used data from the UMass-Stony Brook ^{12}CO survey (Sanders et al. 1986) to estimate the kinetic temperatures of the gas across the 2 deg^2 field. Typical, beam-averaged, line temperatures were $T_{\mathrm{mb}} \sim 8$ K for the lower density clouds and 15 K for the dense regions in the survey field. A beam-averaged line temperature of 10 K is a good approximation of the kinetic temperature for the dark cloud, GRSMC 45.60+0.30, which does not have any star-forming activity. GRSMC 45.46+0.05, however, is a known star-forming region, and it is more likely that the actual kinetic temperatures of the cores of this cloud are higher since they contain embedded heating sources. There-

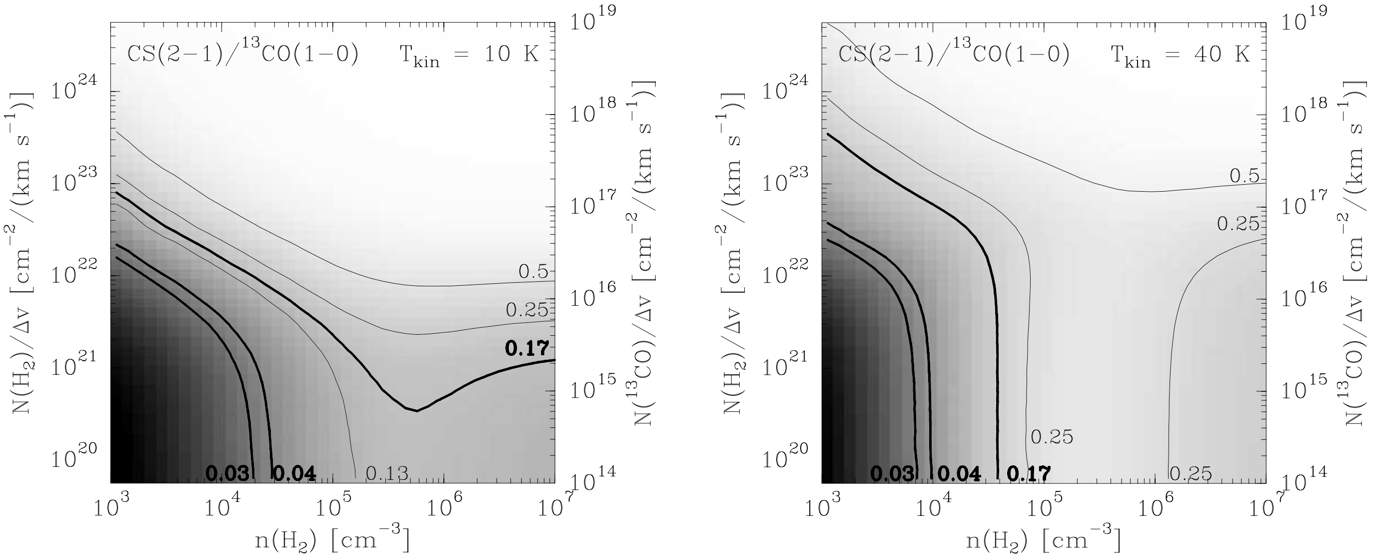

FIG. 11.—Results of a line escape probability model for homogeneous, spherical molecular clouds at two kinetic temperatures: (*left*) 10 K and (*right*) 40 K. Contour lines of constant CS/^{13}CO ratio are drawn. The thick lines represent the observed CS/^{13}CO intensity ratios for the quiescent, low-density molecular cloud GRSMC 45.60+0.30 (0.03), the high-density molecular cores in GRSMC 45.46+0.05 (0.17), and the entire 2 deg^2 region (0.04).

fore, in Figure 11 we present results from the model showing CS/^{13}CO intensity ratios for two kinetic temperatures, 10 and 40 K.

The contour lines of the model CS/^{13}CO ratios show the range of column and volume densities of H_2 that will produce a given intensity ratio. The observed intensity ratios found for the two clouds and the entire field are drawn as thick lines in Figure 11. Although we cannot determine both volume and column densities from just one transition for each molecule, these results do provide a plausibility check on our analysis.

For low values of the CS/^{13}CO ratio (i.e., less than 0.04), high H_2 volume densities are not possible. The average density of regions showing these low values must be much lower than the critical density of the CS transition. As seen in the two panels of Figure 11, the range in plausible densities for this low ratio is only slightly sensitive to the gas temperature. Since the ^{13}CO $J = 1 \rightarrow 0$ transition has a low critical density and is efficiently excited even in very cold gas (the $J = 1$ level is only 5.5 K above the ground state), the CS/^{13}CO ratio in this regime of subthermal excitation of the CS transition is most sensitive to changes in the CS line intensities and hence changes in the volume density. The CS/^{13}CO line ratios increase as the volume density increases.

For H_2 volume densities below the critical density of the CS line and column densities below 10^{21} cm^{-2} (at 10 K) and 10^{22} cm^{-2} (at 40 K), the CS/^{13}CO ratio remains at a constant low level for a given volume density as long as both transitions stay optically thin. For column densities greater than the above values, the CS and ^{13}CO lines rapidly become optically thick.

At densities higher than the critical densities of the transitions, the line intensities for both lines are nearly independent of volume density. Since the critical density of the ^{13}CO $J = 1 \rightarrow 0$ transition is so low, this effect for ^{13}CO already sets in at the lowest volume densities in the plots. It becomes important for CS only at densities higher than $\sim 10^6$ cm^{-3}, where a flattening in particular of the high CS/^{13}CO ratios is evident. Ratio values greater than ~ 0.1 can thus be produced by a wider range of volume densities; the corresponding column densities depend on the temperature of the gas.

The highest ratio found in the survey field, ~ 0.5 at the positions of two CS emission peaks, has a minimum column density of $\sim 10^{22}$ cm^{-2} for 10 K and $\sim 10^{23}$ cm^{-2} for 40 K, but the volume density is not well constrained. The line temperatures necessary to produce the high CS/^{13}CO ratio at high column densities, however, are very high: for a ratio of 0.5 at a volume density of 10^4 cm^{-3} and a column density per velocity interval of 10^{24} cm^{-2}, one would need $T_{\rm mb} \sim 15$ and 30 K for CS and ^{13}CO, respectively. This is not observed. The high values of the ratio are thus plausible only for peak densities of $\sim 10^{5.5}$–10^7 cm^{-3} and column densities greater than 10^{23} cm^{-2}, values that are typical for high-density cores.

In Figure 5, we presented an unbiased average of all 62,000 CS and ^{13}CO spectra and their intensity ratio. We found the mean intensity ratio for the entire survey field to be 0.04 ± 0.01, which is similar to that of the low-density, quiescent molecular cloud GRSMC 45.60+0.30. This confirms the observations by Liszt (1995) that diffuse CS emission is widespread in the inner, northern Galactic plane. Our results from the line escape probability analysis suggest that the H_2 volume density in areas with a low CS/^{13}CO intensity ratio is below the critical density of the CS molecule. Therefore, the ubiquitous and low-level CS emission seen throughout the survey field probably arises from subthermally excited gas.

5. CONCLUSIONS

We mapped 2 deg^2 of the Galactic plane in CS $J = 2 \rightarrow 1$ and ^{13}CO $J = 1 \rightarrow 0$ emission. The maps are fully sampled with high angular and velocity resolution. We compared the emission of these two species and found the following:

1. All regions of bright CS emission, typical of dense molecular cloud cores, also produce bright ^{13}CO emission

because of the large column densities typically associated with the cores. ^{13}CO traces an even higher fraction of *IRAS* point sources satisfying the color criteria for embedded star-forming regions as bright molecular clumps than does CS. Thus, for the purposes of identifying potentially dense and star-forming cores, observations of ^{13}CO are more effective, especially since the stronger ^{13}CO emission is much easier to detect. The intensity ratio CS/^{13}CO is not constant but is a function of gas volume density. We derive this ratio here for high-density CS emission peaks, for a dense star-forming cloud, and for a low-density quiescent cloud.

2. Although the CS molecule is brightest in regions of high volume density, low-level emission from CS is ubiquitous and dominates the total CS intensity averaged over the survey region. The mean of the CS/^{13}CO intensity ratio for all spectra in the 2 deg^2 is similar to the intensity ratio seen toward the lower density molecular cloud studied here. The similarity of the 2 deg^2 average CS/^{13}CO intensity ratio to that of a low-density, quiescent cloud, and the results of radiative transfer models, both suggest that CS emission is dominated by widespread, subthermally excited, lower density molecular gas.

The Galactic Ring Survey acknowledges support by the NSF through grants AST 98-00334 and AST 00-98562. The Five College Radio Astronomy Observatory is supported by NSF grant AST 97-25951. We thank the referee for a careful report that has improved the presentation and the content of the paper.

REFERENCES

Adler, D. S., Lo, K. Y., Wright, M. C. H., Rydbeck, G., Plante, R. L., & Allen, R. J. 1992, ApJ, 392, 497
Blake, G. A., Sutton, E. C., Masson, C. R., & Phillips, T. G. 1987, ApJ, 315, 621
Bohlin, R. C., Savage, B. D., & Drake, J. F. 1978, ApJ, 224, 132
Carpenter, J. M., Snell, R. L., & Schloerb, F. P. 1995, ApJ, 445, 246
Dame, T. M., Hartmann, D., & Thaddeus, P. 2001, ApJ, 547, 792
Drdla, K., Knapp, G., & van Dishoeck, E. 1989, ApJ, 345, 815
Flower, D. R., & Launay, J. M. 1985, MNRAS, 214, 271
Graedel, T. E., Langer, W. D., & Frerking, M. A. 1982, ApJS, 48, 321
Green, S., & Chapman, S. 1978, ApJS, 37, 169
Helfer, T., & Blitz, L. 1997, ApJ, 478, 233
Heyer, M. H., Carpenter, J. M., & Ladd, E. F. 1996, ApJ, 463, 630
Ho, P. T. P., & Townes, C. H. 1983, ARA&A, 21, 239
Jackson, J. M., Bania, T. M., Simon, R., Clemens, D. P., & Heyer, M. H. 2002, ApJ, in press
Jackson, J. M., Heyer, M. H., Paglione, T. A. D., & Bolatto, A. D. 1996, ApJ, 456, L91
Lada, C. J., Alves, J., & Lada, E. A. 1999, ApJ, 512, 250
Lada, C. J., Lada, E. A., Clemens, D. P., & Bally, J. 1994, ApJ, 429, 694
Lada, E., Bally, J., & Stark, A. 1991, ApJ, 368, 432
Langer, W. D., & Penzias, A. A. 1990, ApJ, 357, 477
Lee, Y., Snell, R. L., & Dickman, R. L. 1990, ApJ, 355, 536
Liszt, H. 1995, ApJ, 442, 163
Lockman, F. J. 1989, ApJS, 71, 469
Paglione, T. A. D., Jackson, J. M., Bolatto, A. D., & Heyer, M. H. 1998, ApJ, 493, 680
Paglione, T. A. D., Jackson, J. M., & Ishizuki, S. 1997, ApJ, 484, 656
Prasad, S. S., & Huntress, W. T., Jr. 1982, ApJ, 260, 590
Robinson, B. J., Manchester, R. N., Whiteoak, J. B., Sanders, D. B., Scoville, N. Z., Clemens, D. P., McCutcheon, W. H., & Solomon, P. M. 1984, ApJ, 283, L31
Sanders, D. B., Clemens, D. P., Scoville, N. Z., & Solomon, P. M. 1986, ApJS, 60, 1
Simon, R., Jackson, J. M., Clemens, D. P., Bania, T. M., & Heyer, M. H. 2001, ApJ, 551, 747
Stutzki, J., & Güsten, R. 1990, ApJ, 356, 513
Stutzki, J., & Winnewisser, G. 1985, A&A, 144, 13
Tatematsu, K., Umemoto, T., Heyer, M. H., Hirano, N., Kameya, O., & Jaffe, D. T. 1998, ApJS, 118, 517
Wouterloot, J. G. A., Brand, J., Burton, W. B., & Kwee, K. K. 1990, A&A, 230, 21